03-01

Theoretical examination of semi-implicit time-scheme for nonhydrostatic NWP

Pierre Bénard*, Jozef Vivoda+, Petra Smolikova†, Jan Masek+

* *Centre National de Recherches Météorologiques, Météo-France, Toulouse, France*

+ *Slovak Hydro-Meteorological Institute, Bratislava, Slovakia*

† *Czech Hydro-Meteorological Institute, Prague, Czech Republic*

Severe instabilities were experienced in Aladin-NH (the NH research version of the cooperative NWP LAM model Aladin) when pushing the time-step to values compatible with the implementation of a semi-implicit semi-Lagrangian (SISL) transport scheme in NWP mode. This instabilities were found to be linked to the SI scheme, and to have some similarity with the non-linear instabilities analyzed by Simmons et al., 1978 (SHB78) in the Hydrostatic Primitive Equation (HPE) system. Hence a theoretical study to investigate (and possibly remedy to) this behaviour in the Euler Equations (EE) system was undertaken. The instabilities were successfully reproduced in a framework compatible with theoretical analysis, i.e. linear, resting and isothermal atmosphere. All the analyses are NOT space-discretized, hence the instabilities cannot be suspected to come from some deficient particular choices in the space discretization of the model. Conversely, the framework allows to state on the relevance of other stategic choices: set of prognostic variables, vertical coordinate, time-discretization.

The first simple framework where this instability could be reproduced theoretically was the SHB78 one: when the actual temperature $\overline{T}$ deviates from the SI reference one T^*, for a flat-terrain domain. In this framework, it was proved that the problem is intrinsically due to the original choice for the set of the NH prognostic variables in Aladin-NH, described in Bubnova et al., 1995 (BHBG95). A new set of NH prognostic variables which removed this problem was proposed:

$$\mathcal{P} = \frac{p - \pi}{\pi}$$

$$\mathsf{d} = -g \frac{p}{mRT} \frac{\partial w}{\partial \eta}$$

where p is the pressure, π is the hydrostatic pressure, η is the hybrid hydrostatic-pressure based vertical coordinate (cf: Laprise, 1992), $m = (\partial\pi/\partial\eta)$, and other notations are standard.
With this solution, the stability was proved to be very similar to the one obtained with height-based hybrid vertical coordinates, hence the hydrostatic-pressure-based coordinate has no structural weakness with this respect, compared to height-based coordinates.
It is worth to note that such severe stability problems linked to the choice of the set of prognostic variables were not present in the HPE system, for which the stability of the SI scheme is found to be not very sensitive to the choice of prognostic variables. Another salient result is that even when an optimal choice of prognostic variable is done, the width of the stability domain in the examined context is significantly reduced from HPE system to EE system. The stability domain is $0 < \overline{T} < 2T^*$ for the HPE system and $T^*/2 < \overline{T} < 2T^*$ for the EE system. EE system with SI time-discretization is thus intrinsically less robust than HPE system.

However, in presence of orography, the above proposal was still experienced to induce instabilities, and a framework to better understand the effects of orography hence needed to be examined.

The simple framework where this new instability could be reproduced theoretically consisted in the same as above except that a uniform slope was introduced. This is physically consistent because of the isothermal character of the considered atmosphere, and results in a uniformly slanted coordinate system, which in turn induces additional explicitely-treated terms proportional to the slope in this linear context. In this framework, it was proved that

with the above-mentionned proposal ($\mathcal{P}$, d) for the set of NH prognostic variables, the SI scheme turned unstable again. Finally, a new set of NH prognostic variables which alleviated this problem was proposed:

$$\mathcal{P} = \frac{p - \pi}{\pi}$$
$$\mathsf{d}' = D_3 - \nabla V$$

where D_3 is the 3-dimensional divergence, V is the horizontal wind, and ∇ is the derivative operator along constant η-surfaces. The effect of this new variable is to allow a complete semi-implicit treatment for the acoustic term D_3 which arises due to the compressibility in the pressure and temperature equations.
The analyses showed that the new d′ variable was very beneficial for the stability. However, in contrast with the flat-terrain case discussed above, a residual instability remains even with the new d′ variable. This residual instability of course increases with the slope and the spatial resolution.
This second problem has its exact counterpart in height-based systems, and a similar alleviating solution is traditionnally adopted in models using this vertical coordinate: the vertical velocity w is replaced as a prognostic variable, by a new variable W which also includes the cross term induced in the 3-dimensional divergence by the slanted metrics.

The conclusions that we draw from these analyses can then be formulated as follow: in presence of steep orography and high resolutions, even with a relevant choice of prognostic variables, the SI system as traditionally formulated could be not robust enough to support fully compressible systems. Hence more robust schemes must be examined. The theoretical framework presented here allows to examine the behaviour of such alternative temporal-schemes.

References

Bubnová, R., G. Hello, P. Bénard, and J.F. Geleyn, 1995: Integration of the fully elastic equations cast in the hydrostatic pressure terrain-following coordinate in the framework of the ARPEGE/Aladin NWP system. *Mon. Wea. Rev.*, **123**, 515-535.

Laprise, R., 1992: The Euler equations of motion with hydrostatic pressure as an independent variable. *Mon. Wea. Rev.*, **120**, 197-207.

Simmons, A. J., B. Hoskins, and D. Burridge, 1978: Stability of the semi-implicit method of time integration. *Mon. Wea. Rev.*, **106**, 405-412.

Use of a predictor-corrector scheme to couple the dynamics and physics in the IFS model.

By **Mike Cullen and Deborah Salmond**

European Centre for Medium-Range Weather Forecasts

m.cullen@ecmwf.int, das@ecmwf.int

This work evaluates the performance of an interfacing of the dynamics and physics in the ECMWF model using a predictor-corrector scheme, Cullen (2001). All dynamics and physics terms (except the radiation) are evaluated twice each timestep. Since previous work reported in this publication it has been established that to get stable results it is necessary to use the same spatial interpolation of the physics in both the predictor and corrector steps. In order to get satisfactory performance within the semi-Lagrangian scheme it is necessary to do the interfacing as follows. Consider the simple equation

$$\frac{Du}{Dt} = F + P \tag{1}$$

where F represents the dynamical source terms and P the physics. The corrector step can be represented as the average of two first-order estimates, one of which calculates $F + P$ at each point, and then advects the result, and the other advects values first and applies $F + P$ to the result. The predictor step use the same spatial scheme, but with all values at time t.

$$\begin{aligned} u^* &= u_d^t + \frac{1}{2}\delta t(F_d^t + P_d^t + F_a^t + P_a^t) \\ u^A &= (u^t + \delta t(F^t + P^t))_d \\ u^B &= u_d^t + \delta t(F^* + P^*)_a \\ u^{t+\delta t} &= \frac{1}{2}(u^A + u^B) \end{aligned} \tag{2}$$

Suffices a, d refer to arrival and departure points for the semi-Lagrangian scheme. The equations for u^A, u^B are solved implicitly for the 'fast' parts of the calculation.

Use of this formulation avoids the use of partly updated values in the physical parametrisations, and is consistent with the single column formulation of the physics package. However, it requires the individual parts of the physics to be formulated consistently, with each scheme receiving a profile and a tendency as separate inputs. In the current ECMWF scheme the deep convection does not receive these inputs separately.

The two schemes were tested using 14 forecasts at T_L511L60 resolution run from experimental T511 analyses spread over 18 months between August 1998 and December 1999. The results are shown in Figure 1 . The effect of the predictor-corrector scheme is compared with that of halving the timestep in the operational scheme. The results show that the spread of differences is substantially greater than that given by halving the timestep, suggesting that the formulation changes to the physics allowed by the predictor-corrector scheme have a significant impact.

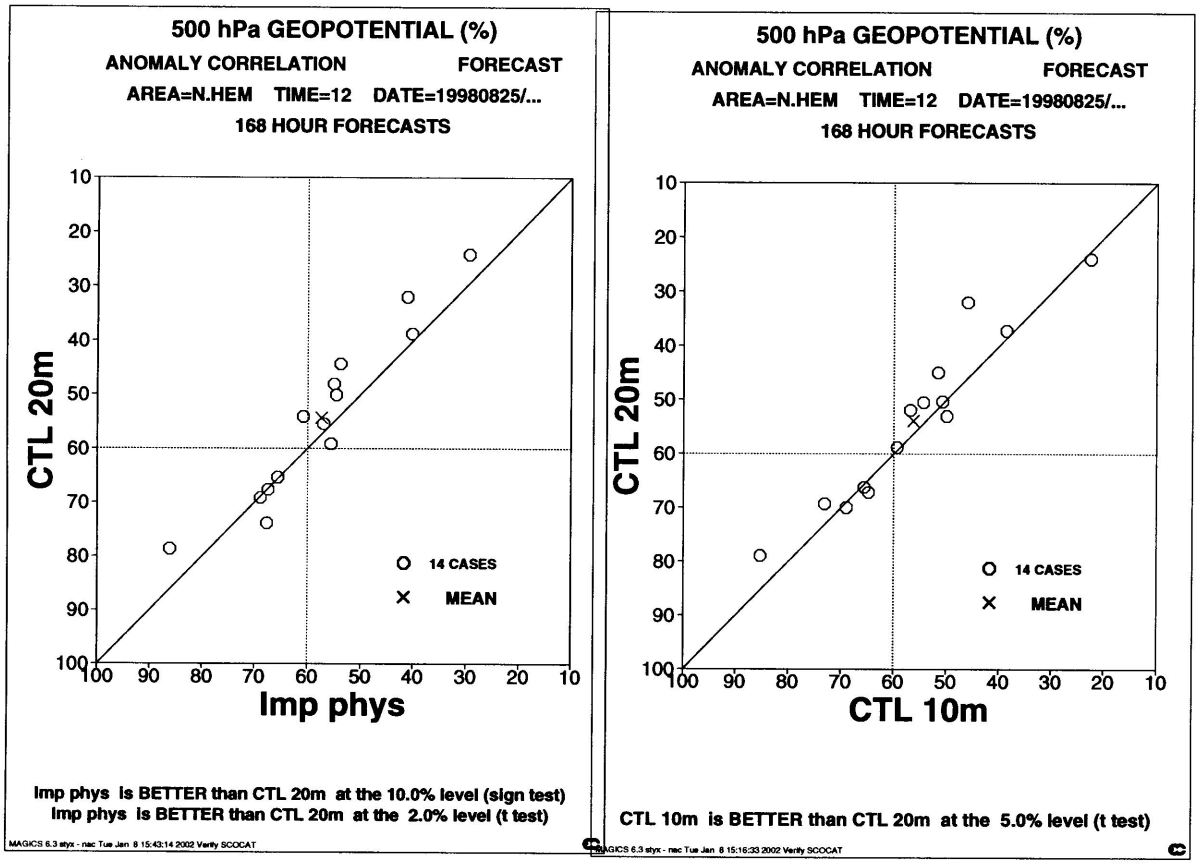

Figure 1 . Scatter plots of 7-day 500hpa geopotential forecasts for 14 cases. Left panel: Control against predictor-corrector (15m timestep) right panel: Control 10 minute timestep against 20 minute timestep

The predictor-corrector scheme reduces the tropical convective precipitation by 10%, which is almost exactly made up by an increase in large-scale precipitation. If the predictor-corrector scheme is iterated a second time, the convective precipitation falls by a further 10% and the total precipitation is decreased by 5%. This illustrates the need to use a formulation of the convection scheme which is consistent with the predictor-corrector scheme.

These results suggest that the predictor-corrector scheme may be a cost-effective way of improving model performance, especially allowing a more satisfactory implementation of the parametrisations. However, all the parametrisations need to be integrated in a consistent way in time. Predictor-corrector schemes may also be a good method for non-hydrostatic models, where the current ECMWF single-step scheme would be unstable.

Cullen,M.J.P. (2001) Alternative implementations of the semi-Lagrangian semi-implicit scheme in the ECMWF model. *Quart. J. Roy. Meteorol. Soc*, **12**, 2787-2802.

Use of potential vorticity as a control variable in a 4DVAR assimilation system.

By **Mike Cullen**

European Centre for Medium-Range Weather Forecasts

m.cullen@ecmwf.int

This note describes experiments to use control variables based on potential vorticity and imbalance to replace vorticity and unbalanced height in the ECMWF data assimilation system. Standard geostrophic adjustment theory shows that the balanced information is carried by the vorticity when the aspect ratio is greater than *f/N*, and by the geopotential otherwise. The present formulation is based on Parrish and Derber (1992) and uses vorticity as the balanced variable, with a linearly balanced height calculated from it and associated temperature and surface pressure deduced statistically. The remaining temperature and surface pressure form the unbalanced variable.

The new formulation is illustrated as follows. Consider the linearised spectral equations for a single zonal wavenumber:

$$\begin{aligned}
&\frac{\partial \zeta}{\partial t} + \mathbf{F}D = \mathcal{Z} \\
&\frac{\partial T}{\partial t} + \tau_r D = \mathcal{T} \\
&\frac{\partial}{\partial t}\ln p_{surf} + \nu D = \mathcal{P} \\
&\frac{\partial D}{\partial t} + \nabla^2(\gamma_r T + \sigma_r \ln p_{surf}) - \mathbf{F}\zeta = \mathcal{D}
\end{aligned} \tag{1}$$

Here, ζ, D, T, p_{surf} represent the vertical component of vorticity, the horizontal divergence, and the temperature and surface pressure. $\mathbf{F}$ is a matrix relating different meridional wavenumbers (the Coriolis parameter), Greek letters represent matrices connecting model levels, and calligraphic letters represent nonlinear terms. The new balance operator can be written as follows for a single vertical mode with gravity wave speed c_n^2 :

$$\begin{aligned}
&(c_n^2 - F\nabla^{-2}F)\zeta_{bn} = Q_n = c_n^2\zeta_n - F\phi_n \\
&(F^2 - c_n^2\nabla^2)\phi_{un} = -c_n^2 R_n = -c_n^2(\nabla^2(\gamma_r T + \sigma_r \ln p_{surf}) - F\zeta) \\
&\nabla^2\phi_{bn} = F\zeta_{bn} \\
&T_n = \tau_r c_n^{-2}\phi_{bn} + T_{un} \\
&\ln p_{surfn} = \nu c_n^{-2}\phi_{bn} + \ln p_{surfun} \\
&\phi_{un} = \tau_r T_{un} + \nu \ln p_{surfun} \\
&\zeta_n = c_n^{-2}\phi_{un} + \zeta_{bn}
\end{aligned} \tag{2}$$

Here the suffices *b* and *u* refer to balanced and unbalanced variables. Q is the potential vorticity appropriate for the linearised equations (1). R is the imbalance. The difficulty with this formulation occurs for modes when $\mathbf{F}$ has a small eigenvalue and c_n^2 is small. This prevents the use of Q_n, R_n directly as control variables. It is found best to use ζ_b, T_u, $\ln p_{surfu}$ as the control variables. Even then, it is necessary to regularise the change of var-

iable either by adding a small term to the left hand side of the first two equations in (2) or by excluding certain modes from the change of variable altogether.

The scheme was still not successful when used with the currently operational form of the ECMWF model on the Lorenz vertical grid. This is because there are many small values of c_n^2. Recently a new vertical formulation has been developed using finite elements, Untch and Hortal (2002), which should become operational early in 2002. This has larger values of c_n^2 for small vertical scales. Results are shown for a 35 day parallel run using the finite-element version of the model and the new balance operator. Each set of forecasts was verified against their own analyses.

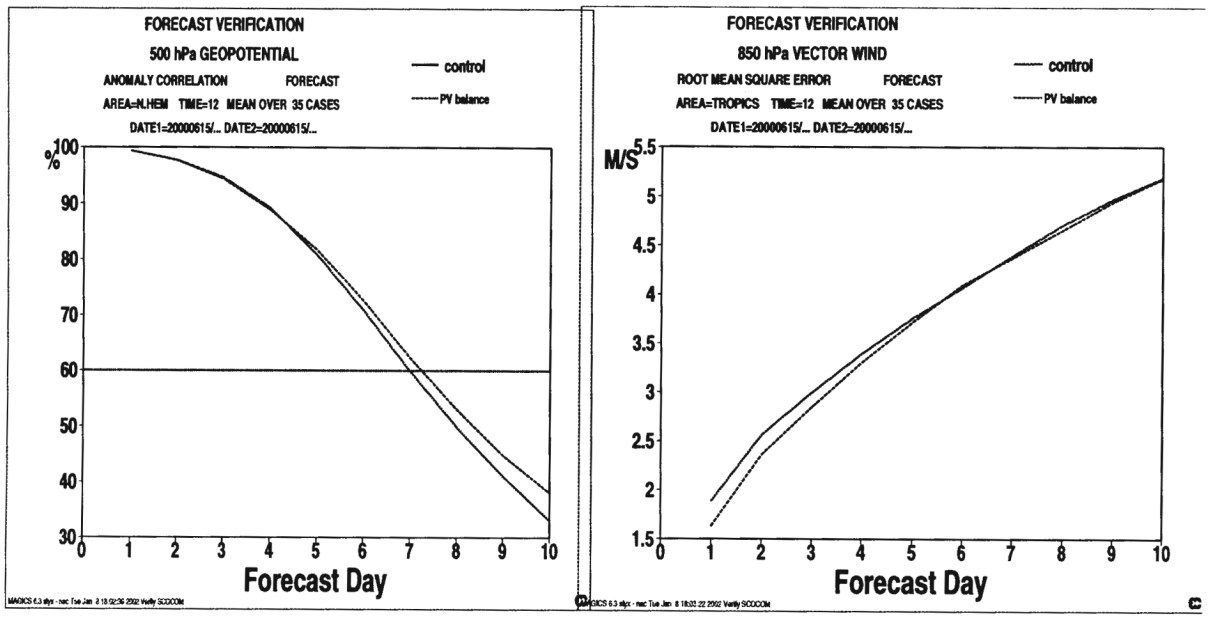

Figure 1 . Left panel: Anomaly correlations for 500hpa forecasts, Northern hemisphere. Right panel: r.m.s. errors of 850hpa wind forecasts for the tropics.

The results show a useful positive impact in the Northern hemisphere. There is also a large positive impact on the tropical wind scores. The latter is because the analyses are significantly smoother, though they verify equally well against observations.

Parrish,D.F. and Derber,J.C. (1992) The National Meteorological Center's spectral statistical interpolation analysis system. *Mon. Weather Rev.*, **120**, 1747--1763

Untch,A. and Hortal,M. (2002) A finite element scheme for the vertical discretisation in the semi-Lagrangian version of the ECMWF forecast model. In preparation.

A two timelevel integration scheme for the nonhydrostatic Lokal-Modell (LM) of DWD

Almut Gassmann, DWD, 63067 Offenbach, Germany
Almut.Gassmann@dwd.de

The current three timelevel integration scheme for the LM has several disadvantages and should be improved or even replaced by an other scheme. The main drawbacks are its low order of approximation for advection, its need for a relatively large number of small time steps for the fast waves integration, its need of the Asselin time filter and its incompatibility to any positive definite advection scheme desired for the moisture variables.

Split-explicit time integration schemes split slow and fast terms of the equations and treat the fast sound and gravity wave terms with a shorter timestep than the others. During this short time step integration, the advective or slow tendency remains a constant. Besides the three time level scheme of Klemp and Wilhelmson (1978)[1] which is used in the operational LM a two timelevel scheme was presented by Wicker and Skamarock (1998)[2]. But this scheme has the disadvantage that it only works in connection with a Runge-Kutta scheme of second order in time and its stability properties are not excellent.

A new scheme works only a bit different than that of Wicker and Skamarock (1998). First, it integrates only the fast wave terms until the center of the time step and one gets result values ϕ^*. Second, from this ϕ^*-values advective tendencies are computed. These might be calculated with any stable two timelevel advection scheme. In a short notation they read as

$$\left(\frac{\partial \phi}{\partial t}\right)_{ADV} = \frac{\phi^{n+1} - \phi^n}{\Delta t} = F(\phi^*).$$

Here $F(\phi^*)$ denotes the advective tendency calculation. In the third step, short time steps are calculated from the beginning of the large time step till its end by retaining the advective tendencies constant. A sketch of this scheme is given in figure 1. The stability analysis of this scheme with different advection algorithms (Runge-Kutta scheme of second order in time, Lax-Wendroff scheme, semi-implicit scheme) shows eigenvalues smaller than one almost everywhere. That means the scheme is stable and reliable.

In the framework of the LM the new scheme needs only 6 short time steps in our configuration (instead of 7 in the current scheme). The Runge-Kutta scheme of second order in time with third order spacial upstream differences is chosen for advection in the horizontal direction. The vertical advection has to be a Runge-Kutta scheme of second order, too. Thereby, centered differences work well and the integration is stable as can be shown by a stability analysis. Third order upstream horizontal differences should also be taken into account for the metric terms appearing in the calculation of the contravariant vertical velocity $\dot{\zeta}$ and of the lower boundary condition for w which is free-slip. Moisture variables are treated with a positive definite van-Leer advection scheme. No horizontal diffusion is added because a slight diffusion effect is present in the advection scheme anyway.

First, ideal 2-dimensional test runs with a dry atmosphere flow over a bell shaped mountain with small scale terrain variations were performed.[3] If the flow field is not exactly balanced, this test fails and a very distorted wave pattern appears, especially in the upper air region. In our simulations, this test performs very well and the result for the w-field (figure 2) is comparable to the analytic solution.

Results of realisic simulations suggest that the scheme is working, but the predicted field of precipitation is noisier in mountainous regions than that of the current scheme (see figure 3). This behaviour is not astonishing, because some of the diffusive and damping mechanisms are no longer present now. May be that other effects as the horizontal transport of precipitation become necessary. Other predicted fields look similar for both runs and stability and performance seem to be satisfactory. There is still work to be done, above all more experiments on realistic cases. All together the two timelevel scheme is promising.

[1] Klemp, J. B. and Wilhelmson, R. B., 1978: The Simulation of Three-Dimensional Convective Storm Dynamics. J. Atmos. Sci., 35, 1070-1096.

[2] Wicker, L. J. and Skamarock, W. C., 1998: A Time-Splitting Scheme for the Elastic Equations Incorporating Second-Order Runge-Kutta Time Differencing. Mon. Wea. Rev., 126, 1992-1999.

[3] as done in Schär, C. et al., 2001: A new terrain-following vertical coordinate formulation for atmospheric prediction models. Submitted to Mon. Wea. Rev.

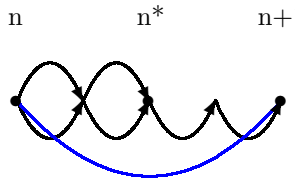

Figure 1: Sketch of the new two timelevel scheme, the line indicates the advection tendency computed of n*, the arrows mark the fast waves computation. ⇑

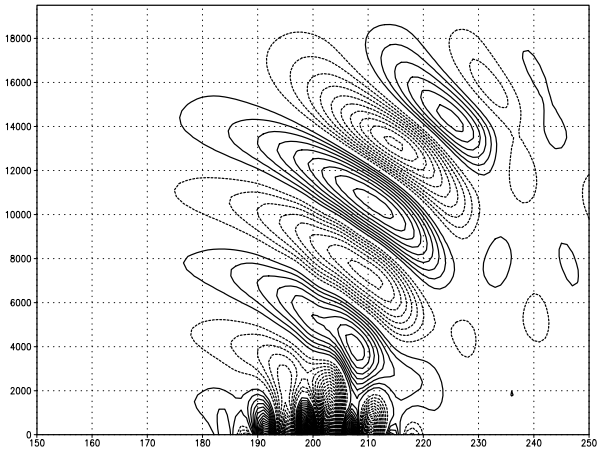

Figure 2: The w-field for the idealized flow over a hilly orography, the contour interval is 0.05 m/s. ⟹

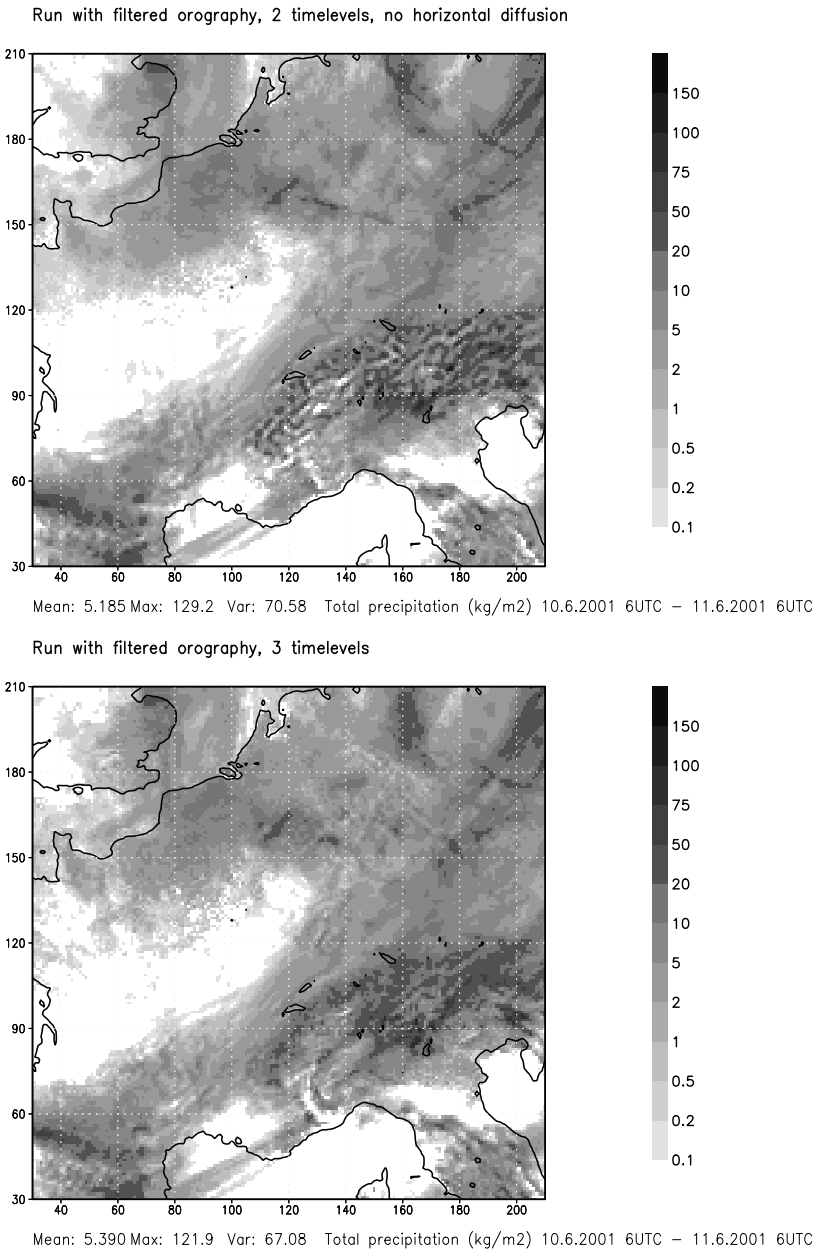

Figure 3: Precipitation pattern for an arbitrary test run wherein the forecasting area includes the Alps. Above: with the two timelevel scheme, below: with the three timelevel scheme

Development of an Ultra High Resolution Global NWP Model

Keiichi Katayama
Numerical Prediction Division, Japan Meteorological Agency
E-mail: k-katayama@naps.kishou.go.jp

1) Introduction

The Japan Meteorological Agency (JMA) has been operating a MPI parallel version of a T213L40 global spectral model (GSM) on the supercomputer HITACHI SR8000E1 since March 2001. GSM supports the official one-week forecast and provides the lateral boundary condition for the JMA Regional models. In order to provide regional scale forecast with a unified model about five years later, we are developing an ultra high resolution GSM which corresponds to a 20km mesh model. We have executed several experimental runs of T319 (38km mesh), T426 (28km mesh), T639 (18km mesh) and T682 (17km mesh) models on the HITACHI SR8000E1.

2) MPI parallel version of JMA GSM

The operational GSM T213 is executed with 16 nodes (PEs) to perform 24-hour forecast within 7 minutes of wall clock. The strategies for parallelization are 1) a simple structure is preferable, 2) instruction loads should be well balanced among nodes, and 3) reproducibility must be guaranteed even if the number of nodes changes. Therefore one-dimensional decomposition in cyclic order is adopted. Fig.1 shows the schematic design of the parallelization. The variable array is decomposed by latitudes in grid space and by zonal wave numbers in spectral space so that all values needed for the summation in both Fourier and Legendre transformations are localized in a node.

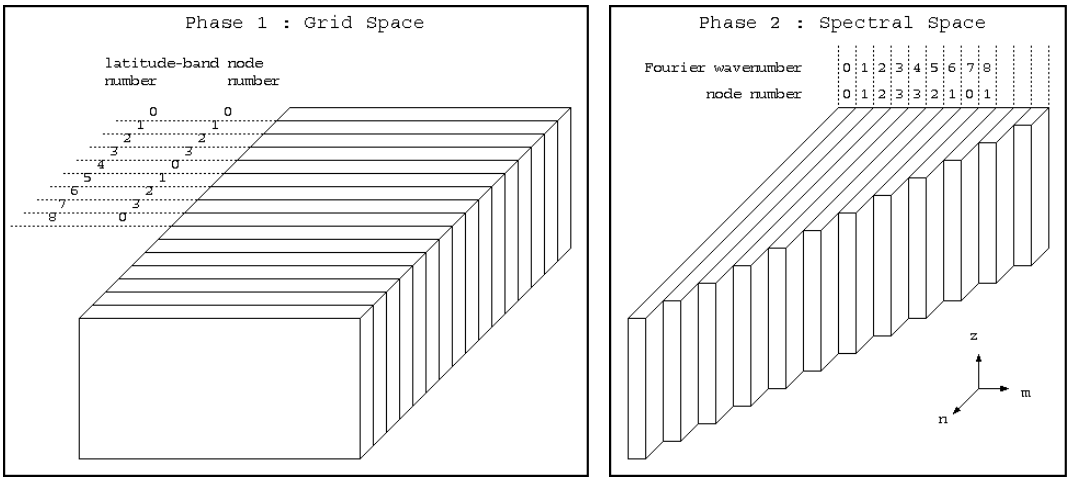

Fig.1 Schematic design of the parallelization.
The number of nodes used is assumed to be 4 in this example.

3) Performance of the Ultra High Resolution GSM

We have executed several experimental runs of T319, T426, T639 and T682 models. T319, T426 and T639 models were computed with 40 nodes, while T682 model was computed with 64 nodes on SR8000E1. Fig.2 shows how computational cost increases as the horizontal resolution increases. T639 takes 32.5 times larger than T213 (ideal computational cost is 3x3x3=27). Fig.3 shows ratio

for execution time in major components of GSM. As the horizontal resolution increases, the ratio of physical process (PHYSCS) is reduced while that of dynamical process (TNDNCY) increases. It should be noted that the moist process (GMOIST) includes both moist physical processes and wave-grid transformation. TINTGS includes the process related to semi-implicit time integration which is computed on wave space. Fig.4 shows the mean sea level pressure and 12-hour precipitation at 48hours forecast with T213, T426 and T682 models. The heavy precipitation around the typhoon T0115 (Danas) is found in T426 and T682 model, and the smaller scale precipitation patterns are found over Japan Island in T682. The central pressure of T0115 in T682 model is 5hPa lower than T213 model.

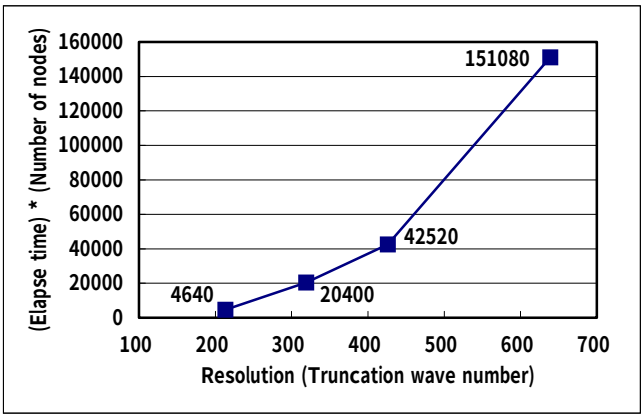

Fig.2 The relation between horizontal resolution (truncation wave number) and total elapse time (in seconds) for 24-hour forecast

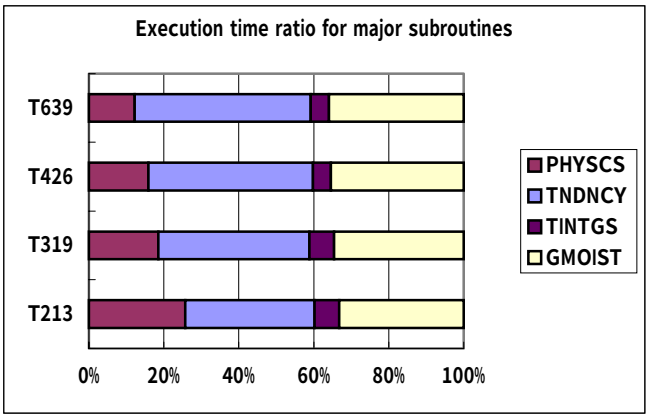

Fig.3 The execution time ratio for major subroutines with different horizontal resolution

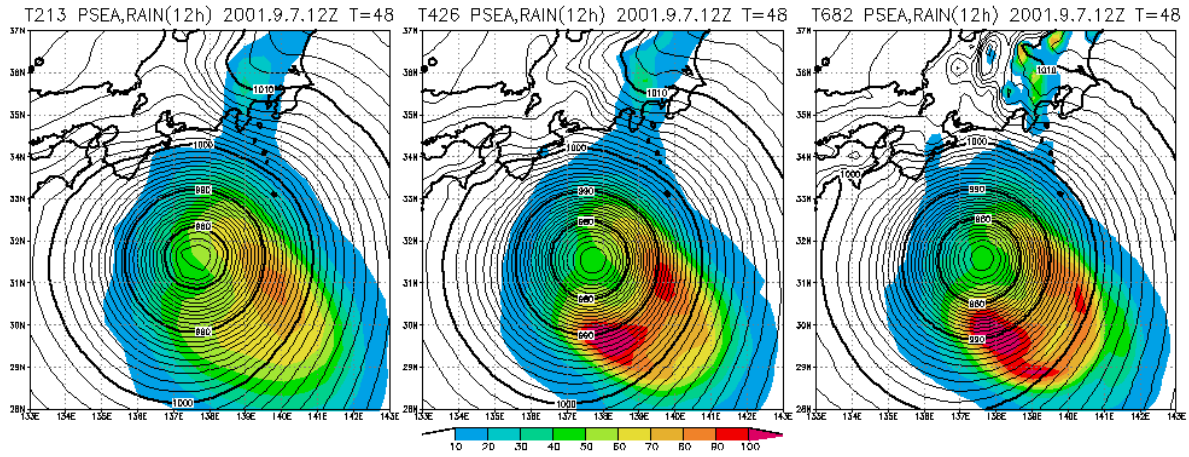

Fig.4 Mean sea level pressure (contour) and 12hour precipitation (shaded) in T213 (left), T426 (middle) and T682 (right) model. 48 hour forecasts of the typhoon T0115 Danas.

4) Future plan

We are trying to execute longer time range forecasts (1-week, 1-month…) with the T682 model, and investigating its forecast fields.

The development of a semi-Lagrangian GSM is also under way at JMA. It is expected that the semi-Lagrangian GSM which corresponds to 20km mesh resolution will be executed on the next JMA supercomputer system.

Comparison of the model climate of various horizontal-resolution

Chiaki KOBAYASHI, Masato SUGI
Climate Research Department, Meteorological Research Institute,
Japan Meteorological Agency
Email: ckobayas@mri-jma.go.jp

A unified NWP-Climate model for operational weather forecasts, seasonal prediction, global warming experiment and for related studies has been developed at Japan Meteorological Agency (JMA) and Meteorological Research Institute (MRI). The unified model is used with different horizontal resolution for various purposes. The recent progress in the high-speed large-memory computer enables us to run the models with very high resolution. However, since a long time-integration with high-resolution model requires a large computer resource, an optimum resolution has to be chosen depending on the purpose. An important question is, therefore, how much the performance of a model is improved by increasing resolution. To investigate the impact of increasing horizontal resolution on the simulated model climate, we conducted an experiment using the JMA operational global atmosphere model (JMA-GSM0103). In the experiment, the model has been integrated for three years with four different horizontal resolutions ranging from T42 to T213 with prescribed climate sea surface temperature.

The distributions of 3-yr averaged seasonal mean precipitation are basically similar among the models with different resolution (Figure 1). The precipitation over equatorial area of the Indian Ocean and the Pacific Ocean in DJF-season tends to be overestimated, particularly in the winter Hemisphere. This error pattern becomes more distinct as the resolution increases. But the differences in seasonal mean precipitation pattern among the models with different resolution are much less than the difference between the model simulation and the observation.

In contrast, smaller scale phenomena are represented better in the high-resolution models as expected. The precipitation band corresponding to Baiu front is seen in the 3-yr averaged monthly mean precipitation pattern for June in the models at all resolution. But the precipitation band of T42 model is located southward of the observation and the amount of precipitation at the peak is less than the observation. The representation of Baiu front is better in the higher resolution models.

Although smaller scale phenomena are represented better in the higher resolution models, the large-scale error patterns of seasonal mean fields are similar among the

models with different resolution. This suggests that the cause of these systematic errors is mainly inadequate representation of physical processes in the model, particularly the tropical precipitation, rather than inadequate resolution. To improve the model climate and its variability, it seems to be more important to improve physical parameterizations, especially convection scheme, than increasing resolution.

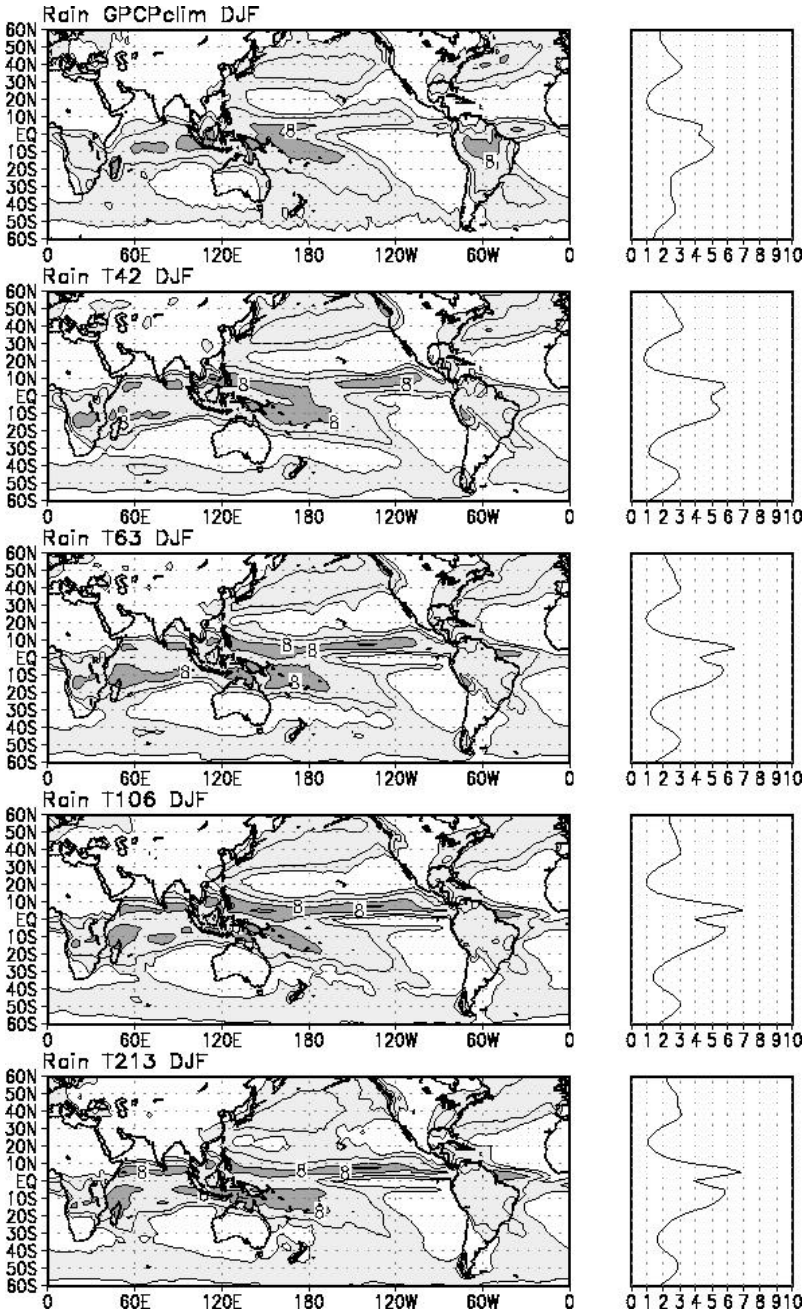

Figure 1 Seasonal mean precipitation in DJF

From top to bottom: GPCP, T42, T63, T106 and T213. Contours : 2,4,8,12 mm/day. Shading: light gray > 2mm/day, dark gray > 8mm/day

Horizontal and Vertical Resolution Dependence of the Representation of a Rapidly Developing Extratropical Cyclone in a Mesoscale Model.

H.W.Lean and P.A. Clark

Met Office JCMM, Reading, UK.

Modelling experiments have been carried out on the FASTEX IOP16 case of a rapidly moving, rapidly developing secondary cyclone. The model used is the new non-hydrostatic version of the Met Office Unified model (Cullen et al 1997**)**. The model has been run for 12 hours in which time the system develops rapidly from two troughs in the original 12km analysis. The development takes place entirely over the ocean which means that all structures smaller than 12km are self generated by the model. The main points of interest in this case are the line convection on the two fronts in the system, multiple cross frontal slantwise circulations and the corresponding multiple cloud head structures. In general the model representation of the system is good. The depth and position of the system are well represented and similar frontal and cloud head features are seen to those in the FASTEX observations (Roberts et. al. 2001).

The model has been run with horizontal gridlengths of approximately 60,24,12,4 and 2km with a level spacing of about 300m in the mid troposphere. This set of runs have been analysed in terms of the isotropic power spectra of their 800hPa vertical velocity fields taken 9 hours into the runs (figure 1). The spectra all tend to the same value at small wavenumbers implying that the large scale structures are similarly represented in all the models (the cut off at small wavenumbers is simply due to the size of the domain used for calculating the spectra). The turn up at the largest values of wavenumber (close to the $2\Delta x$ cut off) in the 24,12 and 4km models is due to the line convection at the fronts since it disappears if the spectra are calculated over an area not including them. The implication is that there is aliasing to the gridscale in all but the 2km model (the 60km model is too low resolution to resolve the line convection).

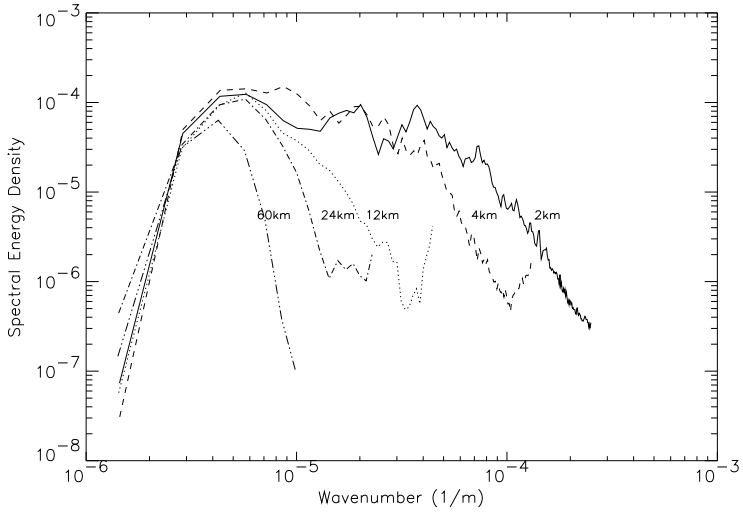

Figure 1. 800hpa Vertical Velocity Power Spectra for various gridlength models

Close examination of the model fields shows that the fronts do, indeed, appear to collapse down to 1 gridlength width in the 24,12 and 4km models but are somewhat broader in the 2km model. The reason for this requires further work. The final interesting aspect of these spectra is the way that the curves decay as the wavenumber increases. In order to

understand this more clearly the same spectra are shown in figure 2 as a fraction of the 2km curve with the wavenumber axis renormalised according to gridlength. These curves represent the way that the response falls off as the wavenumber increases towards the cut off (i.e. as the wavelength reduces towards the 2Δx limit). The four curves lie roughly on top of each other showing that there is a universal fall off in response as the gridlength is approached. It may be seen that the curves start to drop of at roughly 0.1 on the x axis which corresponds to a wavelength of 10Δx. The implication is, therefore, that features seen in the model smaller than around 5 gridlengths are attenuated by the model.

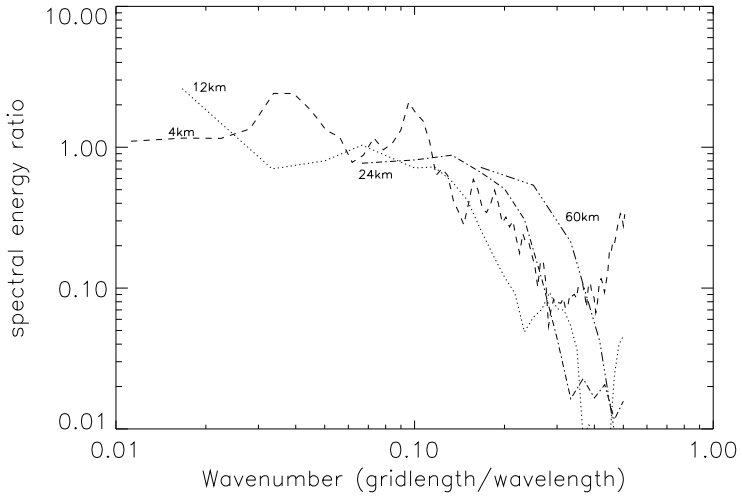

Figure 2. Power Spectra relative to 2km model as described in text

The 4km and 2km models have also been run with the vertical level spacing reduced to 150m and 100m. The representation of the large scale structure of the system with enhanced vertical resolution is unchanged. However the 2km runs with smaller level spacing show additional layering in the cross frontal slantwise circulations which is qualitatively very similar to that observed in the FASTEX dropsonde data. The increased layering looks very similar in the runs with 150 and 100m level spacing in the mid troposphere which implies a degree of convergence with decreasing spacing. The 4km runs, however, show no additional slantwise circulations with increased vertical resolution. The implication is that, at least as far as representation of these types of features is concerned, there is no point in increasing the vertical resolution of the model without also reducing the horizontal gridlength. This fits with the expectation that the aspect ratio of the model grid should be consistent with the slope of the features being represented.

References

Cullen, M.J.P., Davies, T., Mawson, M.H., James, J.A., Coulter, S.C. and Malcolm A., 1997 “An overview of Numerical Methods for the Next Generation UK NWP and Climate Model” Numerical Methods in Atmospheric and Ocean Modelling. The Andre J.Robert memorial volume. Edited by Charles A Lin, Rene Laprise and Harold Ritchie 425-444

Roberts N.M. and Forbes 2001 Submitted to Atmos. Sci. Lett.

Regional climate simulations using a stretched−grid global model

John L. McGregor, Kim C. Nguyen and Jack J. Katzfey

CSIRO Atmospheric Research
PB1 Aspendale, Vic. 3195 Australia

1. INTRODUCTION

Over the last decade, many Regional Climate Model (RCM) simulations have been performed at CSIRO using the Division of Atmospheric Research Limited−Area Model (DARLAM) nested within CSIRO GCM simulations. DARLAM uses fairly conventional one−way nesting at its lateral boundaries, as described by McGregor et al. (1993). More recently, the conformal−cubic global atmospheric model (CCAM) has been developed. This model can be run either in stand−alone mode, or with extra forcing from another simulation provided by far−field nudging of winds. The CCAM simulation described here is of 30−year duration, and uses forcing from the latest CSIRO Mk3 coupled GCM, which has T63 resolution (about 200 km).

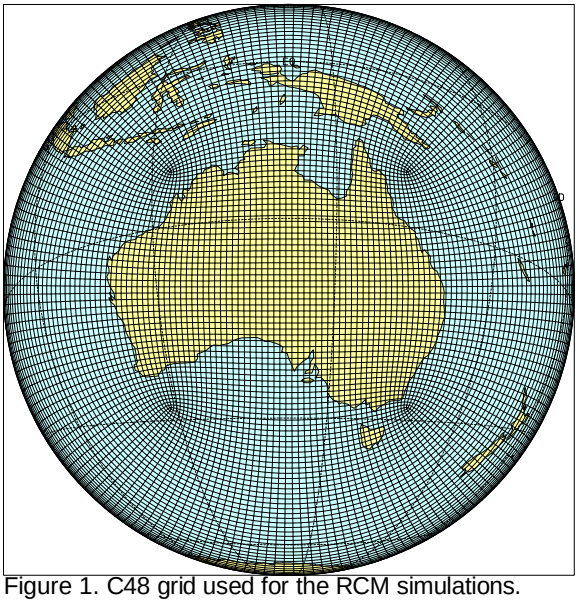

Figure 1. C48 grid used for the RCM simulations.

2. FEATURES OF CCAM

CCAM is formulated on a quasi−uniform grid, derived by projecting the panels of a cube onto the surface of the Earth. CCAM can be run in stretched−grid mode to provide high resolution over any selected region. Compared to the more traditional nested limited−area modelling approach, it provides great flexibility for dynamic downscaling from any global model, essentially requiring only sea−surface temperatures (SSTs) and far−field winds from the host model (McGregor and Dix, 2001). It also avoids other problems that may occur with limited−area models, such as reflections at lateral boundaries.

Distinctive features of the CCAM dynamics include:

- 2−time−level semi−implicit hydrostatic model
- semi−Lagrangian horizontal advection with bi−cubic spatial interpolation
- total−variation−diminishing vertical advection
- unstaggered grid, with winds transformed reversibly to/from C−staggered locations before/after gravity wave calculations
- minimal horizontal diffusion needed:
  - Smagorinsky style used; zero is fine
- Cartesian representation used for:
  - calculation of departure points
  - advection or diffusion of vector quantities
- indirect addressing used to simplify code
- weakly implicit off−centering used to avoid "semi−Lagrangian mountain resonances"
- improved treatment of surface pressure near terrain
- *a posteriori* conservation of mass and moisture.

For the Australian regional climate simulations, the grid shown in Fig. 1 was used, with the following model settings:

- C48 global model (6x48x48 grid points) with 18 vertical levels
- Schmidt stretching factor = 0.3, giving about 65−km resolution over Australia
- nudged by winds from Mk3 CGCM simulation
  - nudged only on furthest panels with e−folding time of at least 24 h.

The latest version of the model includes a new mass−flux cumulus convection scheme, which incorporates downdrafts.

3. RESULTS OF THE SIMULATIONS

Two 30−year RCM simulations were performed with CCAM, with far−field wind forcing supplied by a long transient simulation of the Mk3 CGCM, using the SRES A2 scenario. Sea surface temperatures for the whole domain were supplied twice daily by the CGCM. Results are presented here for the first simulation, which was for present−day greenhouse gas concentrations. The second simulation (not discussed here) was centred around the time of double greenhouse gas concentrations.

The quality of the simulation is illustrated here by showing the average summer rainfall. Fig. 2 displays the observed climatology for December−January−February (DJF) rainfall, as analysed by the Australian Bureau of Meteorology. The high tropical rainfall of the Australian monsoon is evident. Fig. 3 shows the 30−year average of DJF rainfall from the Mk3 CGCM; the broad agreement with the observations is good. Fig. 4 shows the corresponding rainfall from CCAM; the detailed agreement with the observations is even better, with improvements evident over the northern and eastern parts of Australia; the dry interior is also better represented. The CCAM rainfall for the other three seasons (not shown here) also agrees well with the observations.

4. CONCLUDING COMMENTS

Long RCM simulations have been performed for the first time with a stretched global atmospheric model, with far−field nudging supplied by a prior CGCM simulation. The technique is very robust and is capable of providing realistic and detailed climatologies. The technique requires less consistency with the host model, in regard to physical parameterizations, than the traditional one−way nested approach.

REFERENCES

McGregor, J.L., and M.R. Dix, 2001: The CSIRO conformal−cubic atmospheric GCM. In *IUTAM Symposium on Advances in Mathematical Modelling of Atmosphere and Ocean Dynamics,* P.F. Hodnett (Ed.), Kluwer, Dordrecht, 197−202.

McGregor, J.L., K.J. Walsh and J.J. Katzfey, 1993: Nested modelling for regional climate studies. *Modelling Change in Environmental Systems,* A. J. Jakeman, M. B. Beck and M. J. McAleer, Eds., Wiley, 367−386.

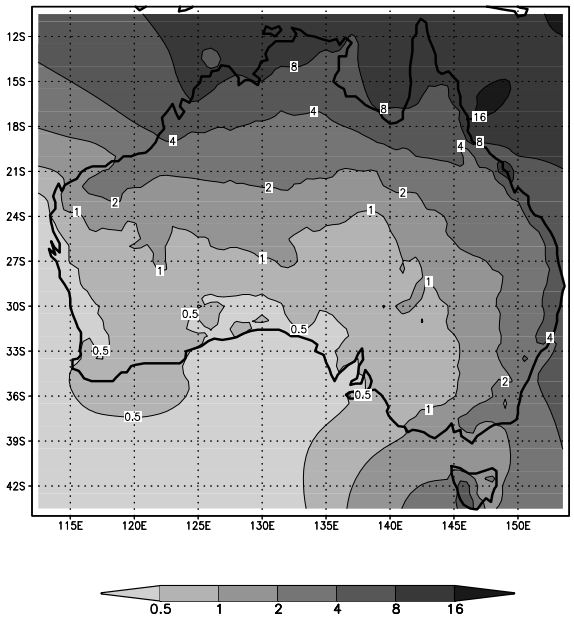

Figure 2. Observed DJF precipitation (mm/day) from the Australian Bureau of Meteorology; all values over the sea should be ignored.

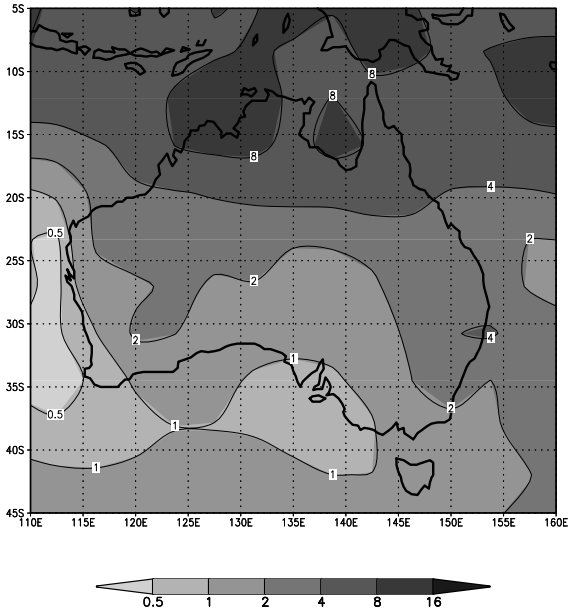

Figure 3. DJF precipitation (mm/day) from the 30−year Mk3 CGCM simulation.

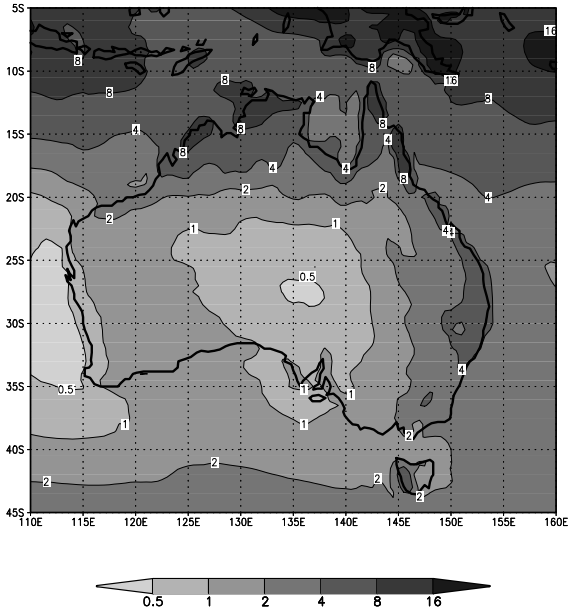

Figure 4. DJF precipitation (mm/day) from the 30−year CCAM simulation.

RMIP simulations with the conformal−cubic model

John L. McGregor

CSIRO Atmospheric Research
PB1 Aspendale, Vic. 3195 Australia

1. INTRODUCTION

Two CSIRO models were used for the Regional Model Intercomparison Project (RMIP): the Division of Atmospheric Research Limited−Area Model (DARLAM), and the Conformal−Cubic Atmospheric Model (CCAM). Both models were run at a resolution of about 60 km over the Asian region from March 1997 to August 1998 with forcing supplied by National Center for Environmental Prediction (NCEP) reanalyses. DARLAM uses fairly conventional one−way nesting at its lateral boundaries, as described by McGregor et al. (1993). In contrast, CCAM is a stretched global model including far−field nudging of winds, temperatures and surface pressure. Several CCAM simulations were performed for RMIP.

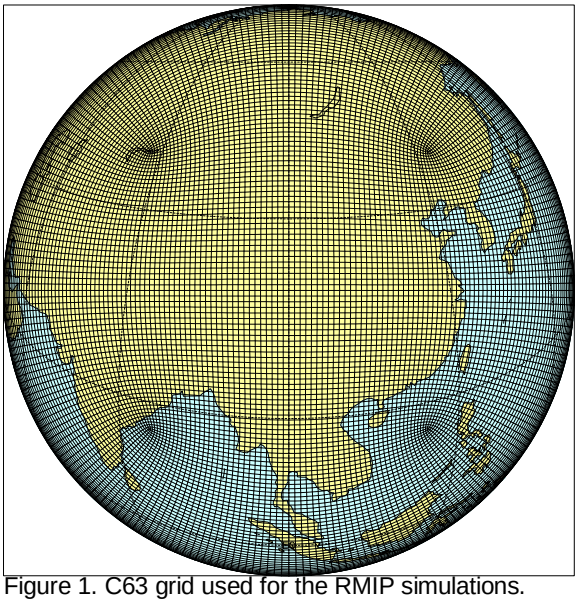

Figure 1. C63 grid used for the RMIP simulations.

2. BRIEF DESCRIPTION OF CCAM

The conformal−cubic global atmospheric model has been developed at CSIRO to augment the regional climate modelling capability provided by the earlier−developed limited−area model (DARLAM). In addition to having a quasi−uniform grid, derived by projecting the panels of a cube on to the surface of the Earth, the conformal−cubic model can be run in stretched−grid mode to provide high resolution over any selected region. Compared to the more traditional nested limited−area modelling approach, it provides greater flexibility for dynamic downscaling from any global model, essentially requiring only sea−surface temperatures (SSTs) and selected far−field variables from the host model (McGregor and Dix, 2001). It also avoids other problems that may occur with limited−area models, such as reflections at lateral boundaries. For the CCAM simulation submitted for RMIP, far−field winds, temperatures and surface pressures were nudged from the NCEP reanalyses for 1997 and 1998. Two experiments are presented here, which include variations on the imposed nudging.

For the RMIP simulations, the grid shown in Fig. 1 was used, with the following model setup:

- C63 global model (6x63x63 grid points) with 18 vertical levels
- Schmidt stretching factor = 0.37, giving about 60−km resolution over Asia
- nudged by 12−hourly NCEP reanalyses
  - nudged only on furthest panels with e−folding time of at least 24 h.

3. RESULTS OF THE SIMULATIONS

Two CCAM simulations are presented here, both using SSTs from the NCEP reanalyses. The simulations use a new mass−flux cumulus convection scheme, which incorporates downdrafts. The simulations are compared here with the observed June−July−August (JJA) precipitation patterns for 1998. Fig. 2 shows the observations, as collated by Xie and Arkin (1997) on a 2.5° latitude/longitude grid.

The first "standard" simulation used far−field nudging of winds, temperatures and surface pressures, as described above. Fig. 3 shows the JJA precipitation pattern, after some 15 months of simulation. There is generally good agreement between the model and the observed fields, although the precipitation seems deficient over northern India, a little deficient over China, and probably excessive over the ocean in the southeast part of the domain. Also, it is a little too dry over southern India, and maybe a little too wet over the Arabian Sea.

The lowest−level model winds may be compared with the 10−m winds from the NCEP reanalyses. The trade winds are generally well captured. The main discrepancies are around Japan and Korea, where the winds have too strong a southeasterly component.

The second simulation used no nudging at all. This simulation also provides a good representation of the JJA precipitation (Fig. 4). Compared to the first simulation, its precipitation is inferior around Korea and the Japan Sea. This simulation is surprisingly good, considering that it did not use any nudging. Shorter simulations centred over Austrlalia (not shown here) exhibited greater sensitivity for the Australian monsoonal rainfall.

A third simulation was also performed, nudging only winds in the far−field. This is the same arrangement used presently at CSIRO for long regional climate runs over Australia, with forcing from the CSIRO coupled GCMs. This simulation produced results (not shown here) fairly similar to those presented above.

It is interesting to display the differences between JJA precipitation in 1998 (when flooding occurred in China) and 1997, for the "standard" simulation. It can be seen from Fig. 5 that there is generally good agreement between the observed and simulated fields. In particular, the increased rainfall over most of China and Korea is well captured, as is the decrease

over Indochina. However, the changes over Japan are not well captured, nor those over India or western China

4. CONCLUDING COMMENTS

The CCAM simulations for RMIP have produced generally good representations of the monsoonal rainfall for 1997 and 1998. The runs use a weaker form of forcing from the analyses than traditional one−way nesting. Perhaps surpisingly, the simulation with zero nudging also produces good monsoonal rainfall; this implies that the monsoonal rainfall over this Asian region is strongly controlled by the SST distribution.

REFERENCES

McGregor, J.L., and M.R. Dix, 2001: The CSIRO conformal−cubic atmospheric GCM. In *IUTAM Symposium on Advances in Mathematical Modelling of Atmosphere and Ocean Dynamics,* P.F. Hodnett (Ed.), Kluwer, Dordrecht, 197−202.

McGregor, J.L., K.J. Walsh and J.J. Katzfey, 1993: Nested modelling for regional climate studies. *Modelling Change in Environmental Systems,* A. J. Jakeman, M. B. Beck and M. J. McAleer, Eds., Wiley, 367−386.

Xie, P., and P.A. Arkin, 1997: Global precipitation: A 17−year monthly analysis based on gauge observations, satellite estimates, and numerical model outputs, *Bull. Amer. Meteor. Soc.,* **78,** 2539−2558.

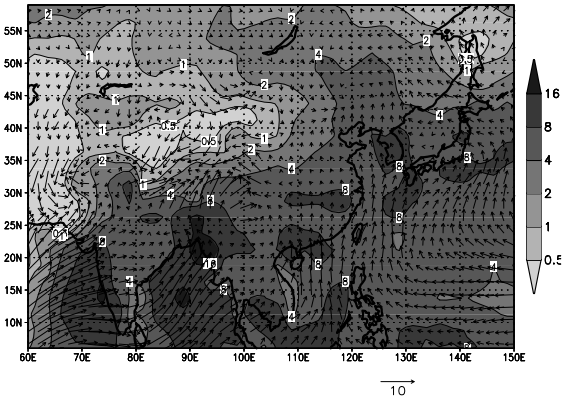

Figure 2. Observed precipitation (mm/day) for JJA 1998 from the analyses of Xie and Arkin, and 10−m winds from the NCEP reanalyses.

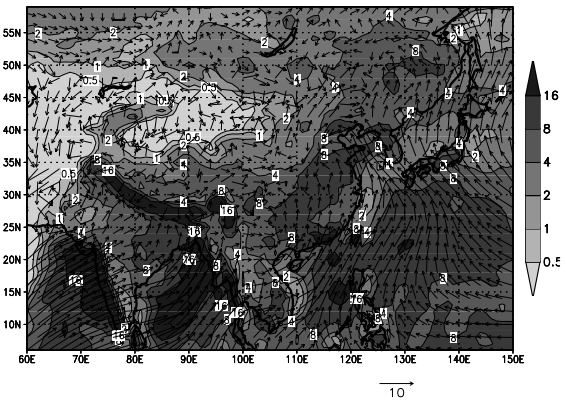

Figure 3. Precipitation (mm/day) and 40−m wind vectors for JJA 1998 from the CCAM simulation with far−field nudging.

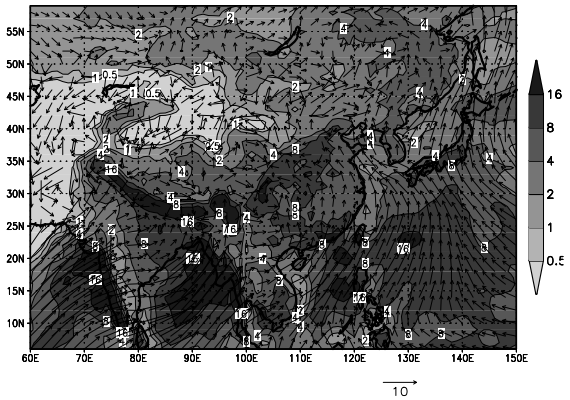

Figure 4. As for Fig. 3, but for the CCAM simulation without any nudging.

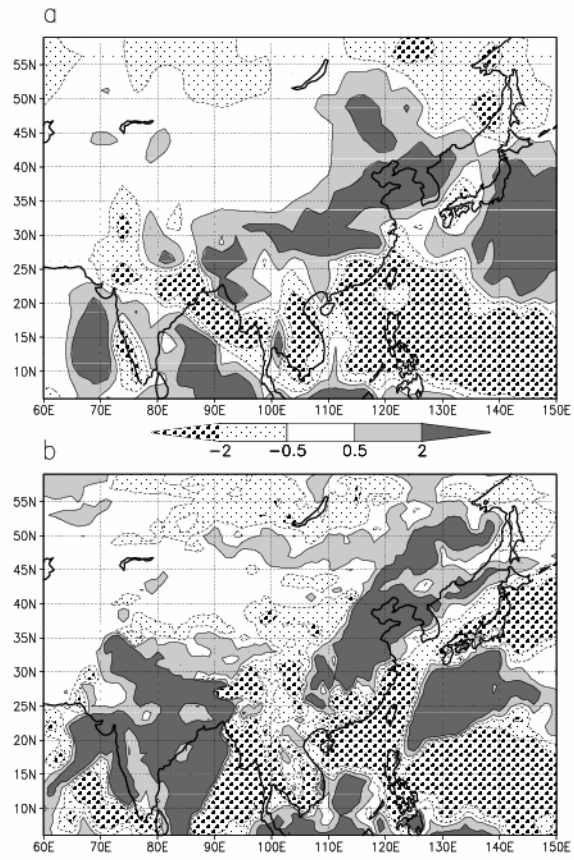

Figure 5. Differences between JJA precipitation (mm/day) over the RMIP region in 1998 from that in 1997 for a) observations, b) the "standard" CCAM simulation.

Should we expect climate models to converge when we increase resolution?

V D Pope and R A Stratton
Met Office, Hadley Centre for Climate Prediction and Research, UK
Email: vicky.pope@metoffice.com

One of the questions that climate modellers should address is whether their models have sufficient spatial resolution to represent the physical processes affecting climate. We have addressed this issue using the Hadley Centre climate model, HadAM3 (the climate version of the Met Office's Unified Model) and report the results in Pope and Stratton (2002). The model is run in AMIP II mode with 4 horizontal resolutions ranging from N48 (2.5 x 3.75 deg) to N144 (0.833 x 1.25 deg). An inherent assumption in this approach, and in numerical modelling of the atmosphere generally, is that models will converge towards an ideal solution as resolution is increased - provided we stay within the range for which the parametrizations are valid. We have shown that this assumption is not always justified. For example, the plot of zonal mean temperatures and differences shows that the warming in the troposphere when resolution is increased is largely converged at N96 (1.25 x 1.875 deg) whereas the cooling around the tropopause at the north pole is only apparent at N144. In principle, undesirable resolution dependencies in physical parametrizations can be removed. However, many processes, and in particular intermittent processes such as convection, are inherently non-linear making resolution dependency inevitable.

We used a range of techniques to identify the processes that affect convergence. For example, dynamical core tests with a smooth uniform land surface everywhere, were used to isolate dynamical processes. 'Spin-up' tendencies were used to diagnose the contribution of individual physical parametrizations and the dynamics scheme. The tendencies are produced by running a series of 1 day integrations starting from operational analyses scattered evenly through the period 1/12/98 to 21/2/99. The analyses use an assimilation system based on the forecast version of HadAM3. Spin-up tendencies are produced by taking the accumulated increments for each of the basic model fields from the dynamics and physical parametrization schemes and averaging them for all the runs. The dependency of the results on particular details of the model were also investigated to see how general the results are.

We showed that non-linearity in both the hydrological cycle and the dynamics play an important role in the lack of convergence. Non-linearity in convection and the response of vertical motion to increased resolution affected the convergence of the tropical circulation, assocated precipitation and the Madden Julian oscillation. They also affected mid-latitude storms. Non-linear dynamics affected the convergence of the tropopause temperature in the full model and the surface pressure in the dynamical core. The general resolution dependency of the results and the particular lack of convergence of some fields mean that it is important to explore the ability of the global model to simulate climate and the signals of climate change at a range of resolutions.

Pope V D and R A Stratton, 2002: The processes governing resolution sensitivity in a climate model. Climate Dynamics, to appear.

Impact of resolution changes on zonal mean temperatures (K)

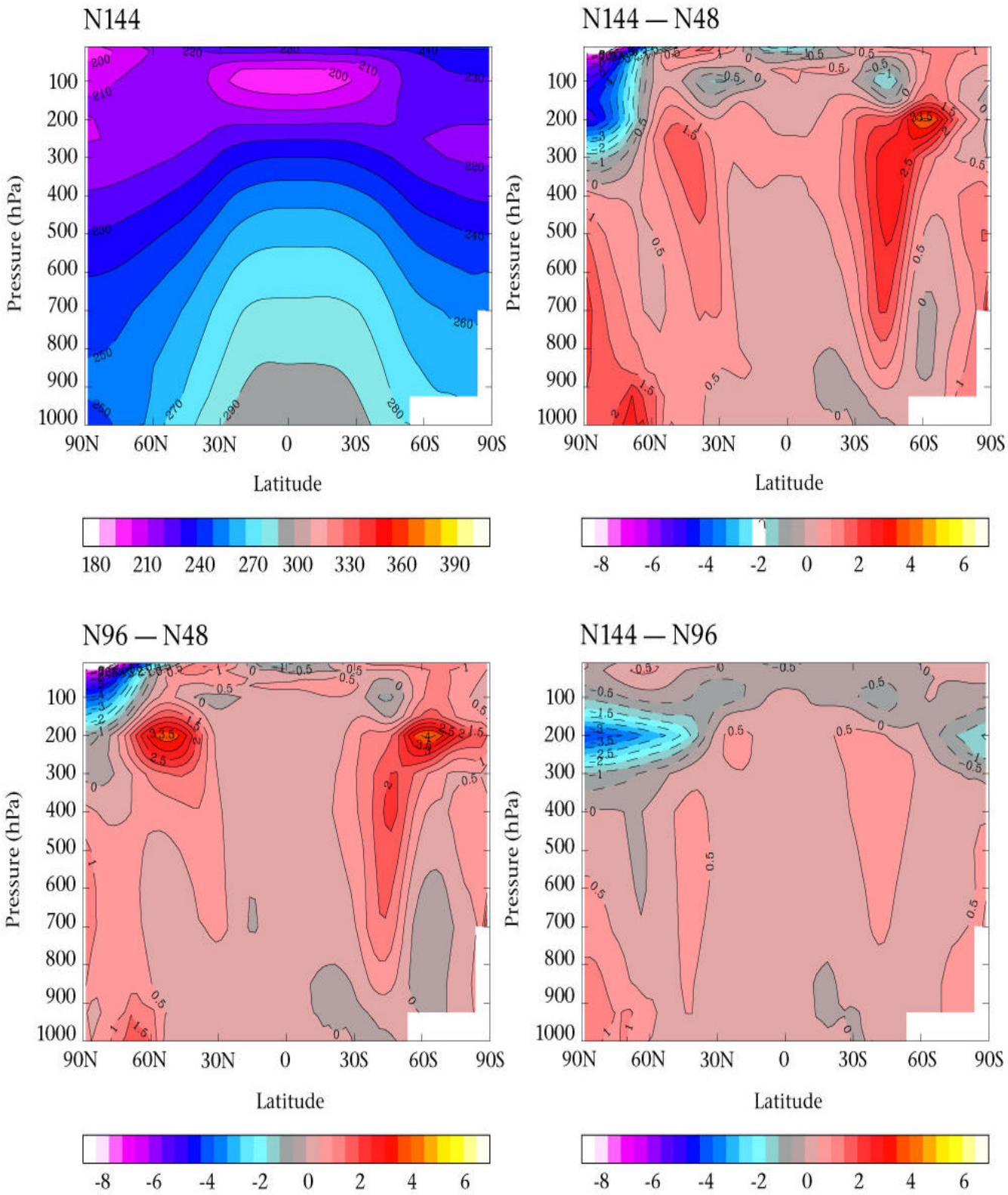

Time-splitting of gravity waves in the Meteorological Research Institute/Numerical Prediction Division unified Nonhydrostatic Model

Kazuo Saito
Numerical Prediction Division, Japan Meteorological Agency, 1-3-4 Otemachi, Chiyoda-ku, Tokyo 100-8122, JAPAN
ksaito@npd.kishou.go.jp

The Japan Meteorological Agency (JMA) started an operational run of a 10 km horizontal resolution mesoscale NWP model in March 2001. The model, MSM, is a high-resolution version of the JMA's operational regional spectral model, where the hydrostatic equilibrium is assumed. As for its initialization, mesoscale 4DVAR is introduced in March 2002. Meanwhile, JMA has a plan to replace MSM by a nonhydrostatic model by the end of FY 2003. Development of an operational nonhydrostatic model for regional NWP (NHM) has been underway, based on the Meteorological Research Institute/Numerical Prediction Division unified nonhydrostatic model (MRI/NPD-NHM; Saito et al., 2001; http://www.mri-jma.go.jp/Dep/fo/mrinpd/INDEXE.htm). Among the three dynamical cores of MRI/NPD-NHM, the Klemp-Wilhelmson type split-explicit time integration scheme (HE-VI scheme) will be used for operation, considering the computational efficiency on the distributed memory parallel computer in the JMA's new NWP system. The HE-VI scheme of MRI/NPD-NHM was incorporated by Muroi et al. (2000), and was based on the formulation of Ikawa (1988). This scheme treats sound waves in the short time step, but has no special treatment for gravity waves. For operational purpose, it is crucial to stabilize the gravity wave modes and remove the dependency of the maximum time step on the atmospheric static stabilities.

The original backward time integrations of the vertical momentum and pressure equations in the HE-VI scheme of MRI/NPD-NHM are written as

$$\frac{W^{\tau+\Delta\tau}-W^{\tau}}{\Delta\tau}+\frac{1}{mG^{\frac{1}{2}}}\frac{\partial P^{\beta}}{\partial z^{*}}+\frac{g}{mC_m{}^2}P^{\beta}=\frac{1}{m}BUOY-(ADVW-RW), \quad (1)$$

$$\frac{P^{\tau+\Delta\tau}-P^{\tau}}{\Delta\tau}+C_m{}^2(-PFT+m^2(\frac{\partial U^{\gamma}}{\partial x}+\frac{\partial V^{\gamma}}{\partial y})$$
$$+m\frac{\partial}{\partial z^{*}}[\frac{1}{G^{\frac{1}{2}}}\{W^{\beta}+m(G^{\frac{1}{2}}G^{13}U^{\gamma}+G^{\frac{1}{2}}G^{23}V^{\gamma})\}]-PRC)=dif.P, \quad (2)$$

where m is the map factor, and terms relating to the tensors for the terrain-following coordinate transformation are represented by $G^{1/2}$, $G^{1/2}G^{13}$ and $G^{1/2}G^{23}$. Terms treated implicitly are indicated with superscripts β and γ. *BUOY* is the buoyancy, *PFT* the thermal expansion of air due to the adiabatic heating, *ADVW* and *RW* are the advection and other residual terms, respectively. *PRC* is the time change of density due to precipitation, and C_m the sound wave speed. To treat the gravity wave modes in the short time step, vertical advection of potential temperature in the basic reference state must be computed in each short time step:

$$\frac{\theta^{\tau+\Delta\tau}-\theta^{\tau}}{\Delta\tau}=-(w^{\tau}\frac{N^2\overline{\theta}}{g}+w\frac{\partial\theta'}{\partial z}+u\frac{\partial\theta}{\partial x}+v\frac{\partial\theta}{\partial y})+\frac{Q}{c_p\pi}+dif.\theta, \quad (3)$$

$$\frac{W^{\tau+\Delta\tau}-W^{\tau}}{\Delta\tau}+\frac{1}{mG^{\frac{1}{2}}}\frac{\partial P^{\beta}}{\partial z^{*}}+\frac{g}{mC_m{}^2}P^{\beta}=\frac{1}{m}\frac{\rho G^{\frac{1}{2}}\theta_m{}'^{\tau+\Delta\tau}}{\theta_m}-(ADVW-RW), \quad (4)$$

where N is the Brunt-Vaisala's frequency. In case of MRI/NPD-NHM, the advection term for potential temperature is written in the flux form as

$$ADV.\theta = \{m^2(\frac{\partial U\theta}{\partial x} + \frac{\partial V\theta}{\partial y}) + m\frac{\partial W^*\theta}{\partial z^*} - \theta DIVT(U,V,W)\}/\rho G^{\frac{1}{2}}, \qquad (5)$$

where $DIVT$ is the total divergence. A flux correction is incorporated as an optional choice to suppress the spurious maxima and minima due to the finite difference and ensure the monotonicity. Besides, computation of the advection term may be further modified in future. In order to utilize the flux form advection Eq. (5), we rewrite Eqs. (3) and (4) as follows:

$$\frac{\theta^{\tau+\Delta\tau} - \theta^{\tau}}{\Delta\tau} = -(w^{\tau}\frac{N^2\bar{\theta}}{g} + w\frac{\partial\theta'}{\partial z} + u\frac{\partial\theta}{\partial x} + v\frac{\partial\theta}{\partial y}) + \frac{Q}{c_p\pi} + dif.\theta$$

$$= -\{\frac{d\bar{\theta}}{dz}(w^{\tau} - w) + ADV\theta\} + \frac{Q}{c_p\pi} + dif.\theta = -\frac{d\bar{\theta}}{dz}(w^{\tau} - w) + \left[\frac{\partial\theta}{\partial t}\right]^*, \qquad (6)$$

$$\frac{W^{\tau+\Delta\tau} - W^{\tau}}{\Delta\tau} + \frac{1}{mG^{\frac{1}{2}}}\frac{\partial P^{\beta}}{\partial z^*} + \frac{g}{mC_m^{\,2}}P^{\beta}$$

$$= \frac{1}{m}\frac{\rho G^{\frac{1}{2}}\theta^{\tau+\Delta\tau}(1+0.61Q_v)(1-Q_c-Q_r-Q_i-Q_s-Q_g)}{\theta_m}g - (ADVW - RW). \quad (7)$$

Here, the second term of *r.h.s.* of Eq. (6) is given by a tentative time integration in the cloud microphysical process, and the first term, which is the vertical advection of the reference state by the difference in w at short and long time steps, is evaluated by the upstream one-sided difference. Since the advection term to compute the tentative time tendency of θ is computed in the flux form, conservation property is kept in the limit where the values of w at short and long time steps coincide.

We also modified the divergence damping filter in NHM to stabilize the sound waves. During the pre-operational test of a 10 km horizontal resolution NHM, no instability for high-frequency modes has been detected using a 40 second long time step increment.

References.

Ikawa, M., 1988: Comparison of some schemes for nonhydrostatic models with orography. *J. Meteor. Soc. Japan*, **66**, 753-776.

Muroi, C., K. Saito, T. Kato and H. Eito, 2000: Development of the MRI/NPD nonhydrostatic model. *CAS/JSC WGNE Research Activities in Atmospheric and Oceanic Modelling*, **30**, 5.25-5.26.

Saito, K., T. Kato, H. Eito and C. Muroi, 2001: Documentation of the Meteorological Research Institute/Numerical Prediction Division unified nonhydrostatic model. *Tech. Rep. MRI*, **42**, 133pp.

A Global Nonhydrostatic Semi-Implicit Semi-Lagrangian Variable Resolution Atmospheric Model

Fredrick Semazzi, George Pouliot & Jeffrey Scroggs
North Carolina State University, Raleigh, NC 27695-8208, fred_semazzi@ncsu.edu

We have replaced the uniform resolution of the global nonhydrostatic semi-implicit semi-Lagrangian (SISL) model described by Semazzi et al (1995) and Qian et al (1998), with a stretched variable grid mesh based on Fox-Robinowitz et al (1997), to investigate the performance of the model in simulating nonhydrostatic motion at sufficiently high spatial resolution.

The core set of simulations consist of three pairs of identical adiabatic twin experiments. Starting from zonal initial motion, disturbances are generated by introducing an isolated meso-scale $(\leq 10km)$ Witch of Agnesi mountain at the bottom of the atmosphere along the equator. For each pair of simulations, a binary switch in the model has been used to suppress or retain the terms in the governing equations responsible for nonhydrostatic dynamics. In these experiments, the spatial and temporal resolution were systematically modified to assess the performance of the global model in reproducing the well known classical orographic meso-scale hydrostatic/nonhydrostatic gravity wave solutions.

In the control pair of identical twin experiments, a modest Courant number of 0.5 $\left(\Delta x = \Delta y = 400m, \Delta t = 10s, and\, U = 20ms^{-1}\right)$ was adopted. The nonhydrostatic version of the model produces the familiar meso-scale stationary gravity wave train anchored to the isolated mountain (bottom panel). The wave has a distinct vertical tilt that is consistent with the classical Long's analytical solutions and with numerical solutions based on limited-area meso-scale nonhydrostatic models. When the nonhydrostatic terms of the model are suppressed, the axis of the resulting gravity wave train rests perpendicular to the mountain top (top panel) thus consistent with the classical theory of meso-scale gravity wave dynamics (Smith 1980). In the second pair of identical twin experiments (figures not shown) the Courant number was increased from 0.5 to 3.0 by changing the time step from 10s to 60s. The corresponding solutions for both the hydrostatic and nonhydrostatic versions of the model are stable although the Courant number significantly exceeds unity. In the third pair of identical twin experiments (figures not shown) the Courant number of 3.0 was retained but the time step was increased from 60s to 300s, and the spatial resolution from 400m to 2,000m. In this case with relatively coarser spatial resolution the solutions are virtually identical for both the hydrostatic and nonhydrostatic versions of the model. Further details about this study may be found in Pouliot et al (2000).

The results show that the performance of the global SISL model is consistent with meso-scale models in the generation of orographically forced hydrostatic and nonhydrostatic gravity waves. This demonstration represents an important step toward the goal of developing efficient multi-scale global nonhydrostatic meso-scale models capable of producing stable solutions at unprecedented large Courant numbers and free of artificial lateral boundary conditions or the need to impose the hydrostatic balance constraint. The computational cost associated with the inclusion of the nonhydrostatic terms in the model is relatively insignificant for the present calculations. The new global scheme is suitable for addressing a variety of unique problems concerning the role of nonhydrostatic dynamics in modulating the global circulation of the atmosphere.

Acknowledgments: This work is partially based on George Pouliot's Ph.D. dissertation. The research was supported by NSF grant#ATM-9119315. The computations were performed on the North Carolina Supercomputing Center (NCSC) IBM SP Power3 computer system. We thank Joshua Qian and Ramachandran Nair for their valuable input.

References

Fox-Robinowitz, M., G. Stenchikov, M. Suarez, L. Takacs, 1997: A finite difference GCM dynamical core with a variable-resolution stretched grid. Mon. Wea Rev. 125, 2943-2968.

Pouliot, G., F.H.M. Semazzi & J. Scroggs, 2002: A global nonhydrostatic semi-Lagrangian atmospheric model with variable resolution. Submitted to MWR. Also see, [climlab4.meas.ncsu.edu/nonhydrostatic2002.html].

Qian, J., F.H.M Semazzi, J. Scroggs, 1998 (QSS98). A global nonhydrostatic semi-Lagrangian atmospheric model with orography, Mon. Wea. Rev., 126, 747-771.

Semazzi, H.F.M., J-H Qian, and J. Scroggs, 1995: A global Semi-Lagrangian Semi-Implicit atmospheric model without orography. Mon. Wea. Rev., 123, 2534-2550.

Smith. R., 1980: Linear theory of stratified hydrostatic flow past an isolated mountain. Tellus, 32, 348-364.

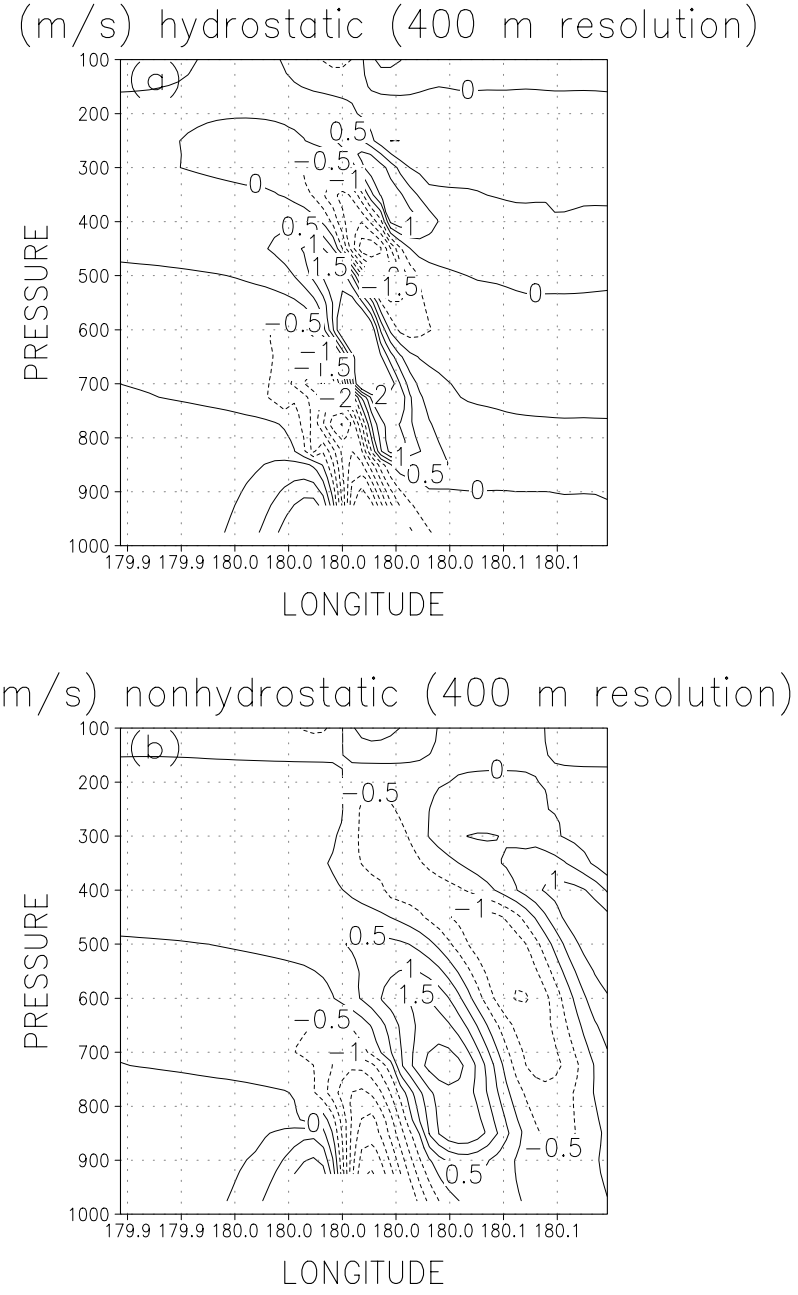

Control case: Idealized orography experiment with, $\Delta x = \Delta y = 400m$, $\Delta t = 10s$, *and* $U = 20ms^{-1}$. Vertical velocity at the Equator (m/s), (a) hydrostatic, and (b) nonhydrostatic after 6 hours. Idealized bell-shaped Witch of Agnesi 3-dimensional mountain with half-width of 2km and maximum height of 500 m. The other two cases are, (i) [$\Delta x = \Delta y = 400m$, $\Delta t = 60s$, & $U = 20ms^{-1}$], and (ii) [$\Delta x = \Delta y = 2000m$, $\Delta t = 300s$ *and* $U = 20ms^{-1}$], and the results are summarized above.

A finite element scheme for the vertical discretization in the semi-Lagrangian version of the ECMWF forecast model

A. Untch and M. Hortal
ECMWF, Shinfield Park, Reading, UK
E-mails: A.Untch@ecmwf.int M.Hortal@ecmwf.int

1 Introduction

The treatment of the vertical part of the gravity wave terms in the forecast equations by means of finite differences in the Lorenz arrangement of variables (hereafter FDL) was the least accurate part of the dynamics of the ECMWF model, being only first order in contrast to the higher order achieved by the spectral discretization in the horizontal and the 3-dimensional semi-Lagrangian advection. To improve its accuracy, a cubic finite element scheme (hereafter FE) for the vertical discretization has been developed and implemented recently in the operational version of the ECMWF analysis/forecast model. The scheme uses cubic B-splines as basis functions. No staggering of variables is required, making it ideally suited for use in conjunction with the semi-Lagrangian advection.

2 Vertical integral operator in finite element representation

In the semi-Lagrangian version of the ECMWF forecast model (see Ritchie et al. 1995) the only vertical operator used is the vertical integral operator.
The vertical integrals involved in the solution of the equations are: 1.) The vertical integral of the continuity equation from the top of the atmosphere to each of the model levels, which gives the vertical velocity needed by the semi-Lagrangian advection and the pressure vertical velocity needed in the thermodynamic equation. 2.) The integral of the continuity equation from the top of the atmosphere to the surface, which gives the tendency of the surface pressure. 3.) The integral of the hydrostatic equation from the surface to each of the model levels.
Integrals starting at the surface can be computed from the corresponding integrals starting at the top of the atmosphere by subtracting the integral from the top of the atmosphere to the surface. Consequently, the only vertical operator needed is the operator "integral from the top of the atmosphere to each of the model levels and to the surface".
This vertical integral operator has been evaluated in finite element representation by using cubic B-splines as basis functions with compact support (Prenter, 1975, and references therein) and by applying the Galerkin method. We incorporated the transformations to spline space and back to physical space into the operator to obtain a matrix which operates in physical space, i.e. when applied to a function given on model levels (plus appropriate boundary conditions), the operator yields the values of the integral of this function on model levels.

3 Results

The new FE scheme has been tested extensively in runs with the dynamical core version of the model as well as with the full model in data assimilation and forecast mode. The main benefits we have found are:
1.) The vertical linear gravity eigenmodes computed with the FE scheme are more similar than the FDL ones to the eigenmodes obtained with finite differences in Charney-Phillips arrangement. The latter arrangement of variables is ideally suited to the treatment of the gravity wave terms in the forecast equations and is free of the spurious computational mode in the vertical present in the

FDL, but it is more difficult to use in conjunction with semi-Lagrangian advection due to the staggering of temperature and winds. The FE scheme improves on the treatment of the gravity wave terms while retaining the advantage for the semi-Lagrangian scheme of not having staggered variables.

2.) The FE scheme reduces substantially the amplitude of the small scale vertical structures produced in divergence (mainly in the tropical stratosphere) with the FDL scheme.

3.) This noise reduction in divergence, together with the improved vertical integration of the continuity equation with the FE integral operator, leads to a more accurate computation of the vertical velocity which in turn improves the semi-Lagrangian advection in the vertical. As a consequence, tracer conservation in the semi-Lagrangian model is improved with the FE scheme. Fig. 1 shows the percent change in global ozone mass in two ensembles of 60-day forecasts (with the ozone chemistry switched off) run with the FE scheme (dashed line) and with the FDL scheme (control runs). With the FE scheme the lack of conservation is reduced by about 50%.

4.) In data assimilation, a better fit of the first guess to radiosonde data in the lower stratosphere is found with the FE scheme, resulting in the use of more observations in the analysis.

5.) The FE scheme also gives a substantial improvement in stratospheric skill scores, notably in RMSE of temperature in the tropics.

4 References

Prenter, P. M., 1975: Splines and variational methods, *John Wiley& Sons*.

Ritchie H., C. Temperton, A. J. Simmons, M. Hortal, T. Davies, D. Dent, M. Hamrud, 1995: Implementation of the semi-Lagrangian method in a high-resolution version of the ECMWF forecast model, *Mon. Wea. Rev.* **123**, No 2, 489-514.

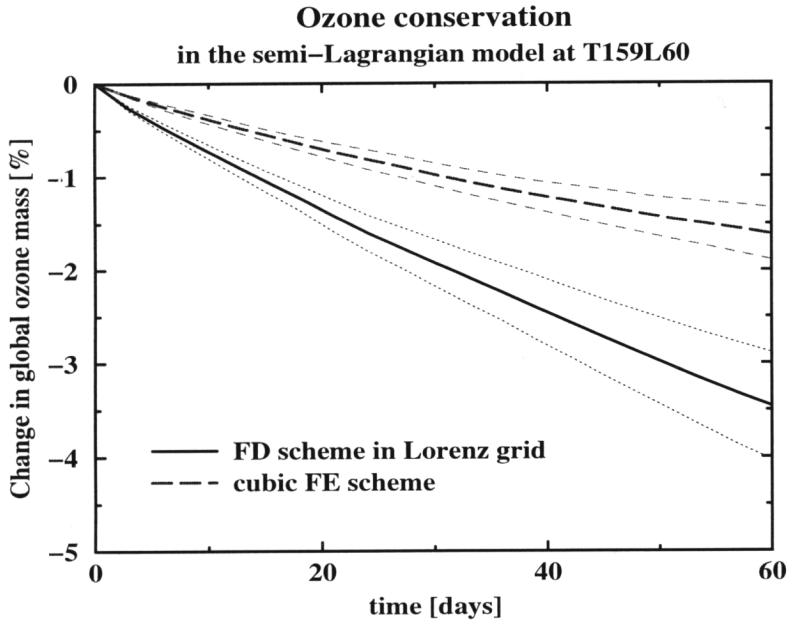

Fig. 1 Percent change of global ozone in two ensembles of 60-day forecasts using the cubic finite element scheme (dashed line) and the finite difference scheme in Lorenz arrangement (control) (full line). The thick lines are the mean and the thin lines give an indication of the spread ($mean \pm stdev$).